http://dx.doi.org/10.5012/bkcs.2012.33.2.529

DNA Mediated Energy Transfer from 4',6-Diamidino-2-phenylindole to *tetra*- and *bis*-cationic Porphyrins at Low Binding Densities

Lindan Gong, Jae Ki Ryu,[†] Bok-Jo Kim,[‡] and Yoon Jung Jang[*]

Department of Chemistry, Yeungnam University, Gyeong-buk 712-749, Korea. [*]E-mail: jyj5014@ynu.ac.kr
[†]Department of Biomedical Laboratory Science, Gimcheon University, Gyeong-buk 740-704, Korea
[‡]Department of Biomedical Laboratory Science, Gyungwoon University, Gyeong-buk 742-711, Korea
Received October 24, 2011, Accepted December 8, 2011

The fluorescence of 4',6-diamidino-2-phenylindole (DAPI) bound to DNA at a [DAPI]/[DNA base] ratio of 0.005 was quenched by *meso*-tetrakis(*N*-methylpyridinium-4-yl)porphyrin (TMPyP) or *cis*-*bis*(*N*-methylpyridinium-4-yl)porphyrin (BMPyP) when both DAPI and either porphyrin spontaneously bound to the same DNA strand. The quenching was investigated using the "one-dimensional inner sphere" and the "Förster resonance energy transfer" (FRET) models. Total quenching occurred when DAPI and TMPyP were up to 19.3 base pairs or 66 Å apart. BMPyP could quench the fluorescence up to 13.9 base pairs or 47 Å. TMPyP, which intercalated between the DNA base-pairs, appeared to be a better acceptor than BMPyP, which stacked along the DNA stem. The higher quenching and higher resonance energy transfer efficiency of TMPyP was due to the larger overlap integral between its absorption spectrum and the emission spectrum of DNA-bound DAPI.

Key Words : Energy transfer, 4',6-Diamino-2-phenylindol, Porphyrin, DNA, Fluorescence

Introduction

DNA has been an interesting subject for generations of biological, chemical, and physical scientists as the vehicle for inheritance in cellular life. Understanding the processes that damage DNA and cause mutations takes on great importance for this reason. Energy and charge transfers between DNA-bound or free drugs to DNA bases can damage DNA, with the stacked π-orbitals of the DNA base pairs forming a good medium of energy transfer,[1] which frequently occurs with the transfer of electrons.[2-6] One of the first examples of electron transfer along DNA involved metallo-intercalators non-covalently bound to DNA. DNA mediated hole transfer has also been studied, because holes can oxidatively damage DNA damage *in vivo*, leading to mutations. Holes generated by the one-electron oxidation of DNA can travel over 200 Å through the DNA by hopping between guanine bases.[7-13] The biological importance of charge transport through DNA has been highlighted by the discovery of distance oxidative DNA damage in cell nuclei.[14,15] The concepts of DNA-mediated charge transport could also aid the development of nanodevices, e.g. the design of nanometer-sized self-assembling molecular wires.[16-19]

The excited energy of DNA-bound donors can transfer to acceptors.[20-29] Generally, the emission energy level of a donor molecule coincides with the absorption energy level of the acceptor, in the DNA mediated excited energy transfer, thus, is resonance energy transfer (RET) type in its nature. The excited energy of 4',6-diamidino-2-phenylindole (DAPI, Figure 1) has been reported to transfer to DNA intercalating [Ru(1,10-phenanthroline)$_2$dypyrido[3,2-*a*:2'3'-*c*]phenazine]$^{2+}$ at high binding densities.[24-27] The DAPI donor binds at the minor groove of DNA[30-32] and the acceptor intercalates at the major groove as DAPI saturates the minor groove. Therefore, energy transfers across the DNA stem. The intercalating acceptor *meso*-tetrakis(*N*-methylpyridinium-4-yl)porphyrin (TMPyP, Figure 1) facilitates more efficient energy transfer from DAPI than that predicted by the "sphere of action model".[28,29] Important factors that affect the efficiency of RET include spectral overlap and the relative orientation of the donor and the acceptor molecules.[33] *Cis*-*bis*(*N*-methylpyridinium-4-yl)porphyrin (BMPyP, Figure 1) has been reported to stack along DNA.[34,35] Their different binding modes to DNA allow investigation of the effects of spectral overlap and relative orientation in RET. DAPI was used at a concentration ratio to DNA bases of 0.005, one DAPI molecule per 200 bases. Such low binding density

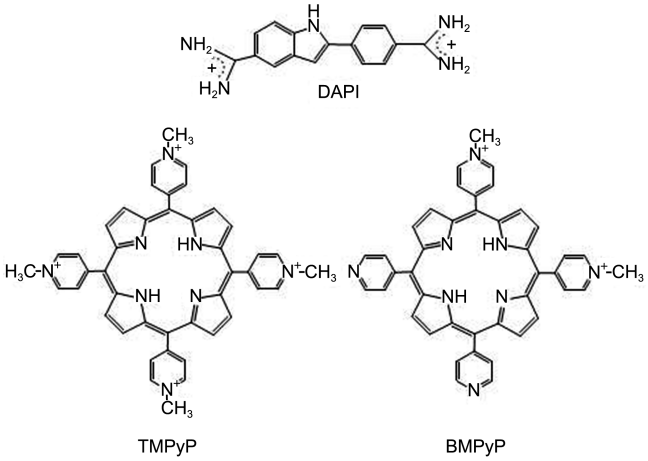

Figure 1. Chemical structure of 4',6-diamidino-2-phenylindole (DAPI), *meso*-tetrakis(*N*-methylpyridinium-4-yl)porphyrin (TMPyP) and *cis*-*bis*(*N*-methylpyridinium-4-yl)porphyrin (BMPyP).

avoids direct contact between DAPI and the porphyrins.

Experimental

Materials. Calf thymus DNA (Sigma-Aldrich, Seoul, Korea) was dissolved in 5 mM cacodylate buffer and used without further purification. TMPyP, BMPyP (Frontier Scientific, Logan, UT) and DAPI (Sigma-Aldrich) were used without further purification. Concentrations were spectrophotometrically determined using the extinction coefficients: A_{258nm} = 6700 $cm^{-1}M^{-1}$, A_{342nm} = 27000 $cm^{-1}M^{-1}$, A_{421nm} = 245000 $cm^{-1}M^{-1}$ and A_{420nm} = 140000 $cm^{-1}M^{-1}$ for DNA, DAPI, TMPyP and BMPyP, respectively. The porphyrins were always added last, immediately before measurement, as the mixing order can affect their binding mode.[36]

Measurements. Absorption and circular dichroism (CD) spectra were recorded using a Cary 100 spectrophotometer (Varian, Palo Alto, CA) and a Jasco J710 spectropolarimeter (Tokyo, Japan), respectively. Fluorescence intensities were measured on a Jasco FP-777 spectrofluorometer. During titration of the DAPI-DNA complex by porphyrins, small aliquots of the latter were added to the sample solution and volume corrections were made. The emission intensity of DAPI was monitored using excitation at 360 nm and emission at 450 nm. These wavelengths allowed changes in DAPI fluorescence to be monitored without interference from the porphyrins' fluorescence. The fluorescence decay time of DAPI was measured using an IBH 5000U Fluorescence Life Time System. An LED source (nano-LED-03) produced 360 nm excitation radiation with full width at a half-maximum of ~1.3 ns to excite the DNA-bound DAPI. Slit widths of 32 nm were used for both excitation and emission.

Results

Absorption and CD Spectra of Porphyrins Bound to DNA in the Presence and Absence of DAPI. Figures 2(a) and 2(b) respectively show absorption spectra of 2.5 mM TMPyP and BMPyP bound to DNA. The presence of DAPI did not alter the spectra, suggesting that it did not affect the porphyrins' binding modes. Spectra recorded at porphyrin concentrations of 0.5, 1.0, 1.5 and 2.0 μM were identical when normalized with respect to concentration and are hence not shown. The binding of TMPyP to DNA resulted in large, 37.7%, hypochromism with a 19 nm red shift compared with that in the absence of DNA. BMPyP's absorption spectrum showed a red shift of 9 nm with 32.4% hypochromism, in accordance with previous results,[34] indicative of the molecules' different binding modes. Achiral porphyrins can induce CD signals, particularly in the Soret absorption region, upon binding to DNA due to the interactions of B_x and B_y electric transitions and the chirality of the DNA bases' electric transition moments. The shape of the induced CD in the Soret region reflects the porphyrin's binding mode. Upon binding to DNA, TMPyP produced a negative CD band and no CD signal was observed for BMPyP, as reported elsewhere.[34] These CD signals represent the intercalation of TMPyP and the binding of BMPyP outside the DNA stem, possibly stacking along it. The presence of DAPI at the low binding density used here did not alter the shape of either porphyrin's induced CD spectrum. This indicates that the binding of DAPI at DNA's minor groove did not affect the binding mode of either porphyrin (Figure 3).

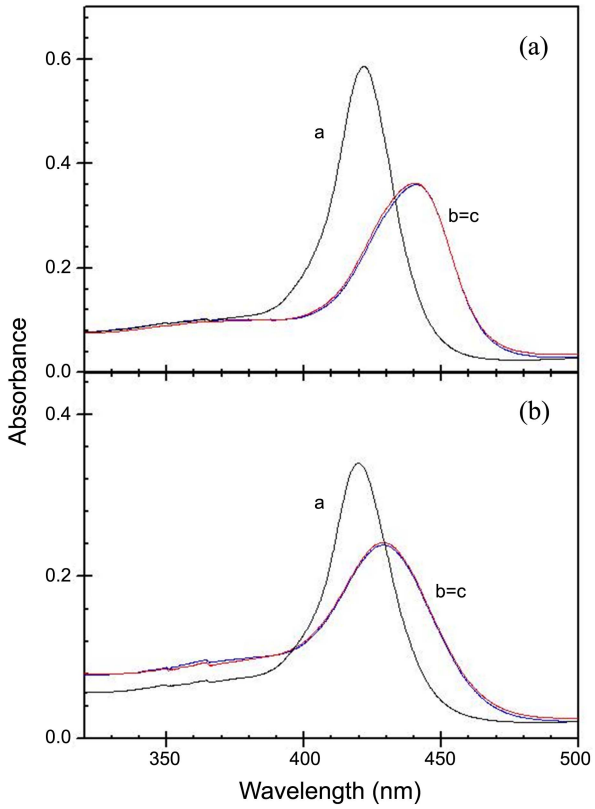

Figure 2. Absorption spectra of TMPyP (panel a) and BMPyP (panel b) in the absence (curve a) and presence (curve b) of DNA. The presence of DAPI did not alter the porphyrins' absorption spectra (curve c). [DNA] = 100 μM, and [porphyrin] = 2.5 μM.

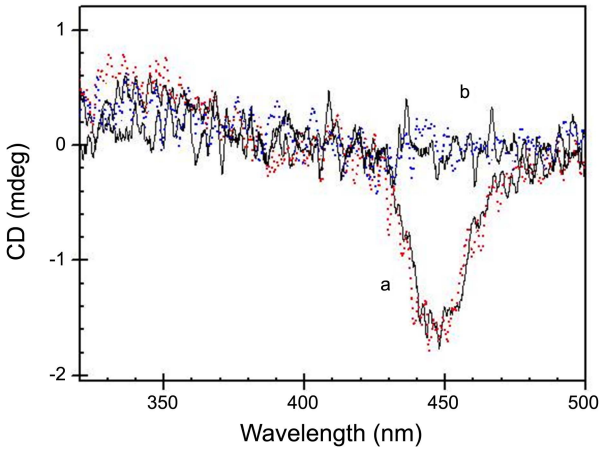

Figure 3. CD spectra of DNA-bound TMPyP (curve a) and BMPyP (curve b). The presence of DAPI did not affect the CD spectra (dotted curves). Concentrations are as per Figure 2.

Quenching of DAPI Fluorescence by Porphyrins. The fluorescence intensity of DNA-bound DAPI gradually decreased with increasing porphyrin concentration (Figure 4).

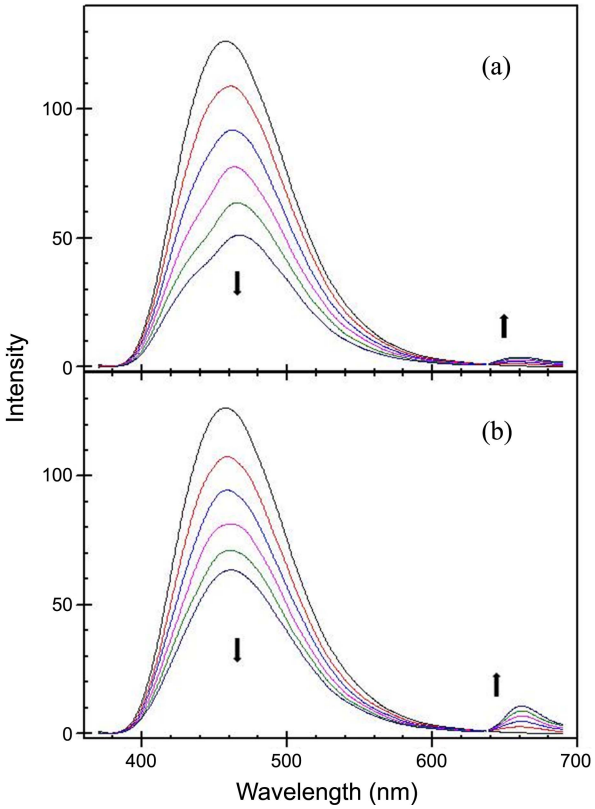

Figure 4. Fluorescence emission spectra of DAPI bound to DNA with increasing concentrations of TMPyP (panel a) and BMPyP (panel b). [DNA] = 100 μM, [DAPI] = 0.5 μM. Porphyrin concentrations of 0, 0.5, 1.0, 1.5, 2.0 and 2.5 μM were testing, increasing in the direction of arrow. DAPI-DNA complexes were excited at 360 nm and 5 nm slit widths were used for both excitation and emission.

The decrease was more pronounced with TMPyP. The decrease in the emission at *ca.* 460 nm was accompanied by a small increase in emission near 660 nm, attributable to the porphyrins emitting their excitation energy. This increase of fluorescence was more pronounced with BMPyP. Fluorescence quenching can be analyzed through Stern-Volmer plots,[33] in which the ratio of fluorescence intensity in the absence of quencher to in its presence is plotted with respect to the concentration of quencher:

$$\frac{F_0}{F} = 1 + K_{SV}[Q] \quad (1)$$

Where F_0 and F denote the fluorescence intensities of the fluorophore (here DNA-bound DAPI) in the absence and presence of quenchers, respectively. [Q] is the concentration of quencher (here TMPyP or BMPyP). The quenching constant, K_{SV}, represents the equilibrium constant for the formation of nonfluorescent fluorophore-quencher complexes in the static quenching process. In the dynamic-collision quenching mechanism, the quenching constant is related to the frequency of collisions and the lifetime of the excited state of the fluorophore. Upward bending Stern-Volmer plots were observed for both TMPyP and BMPyP; TMPyP showed more efficient fluorescence quenching (Figure 5). The

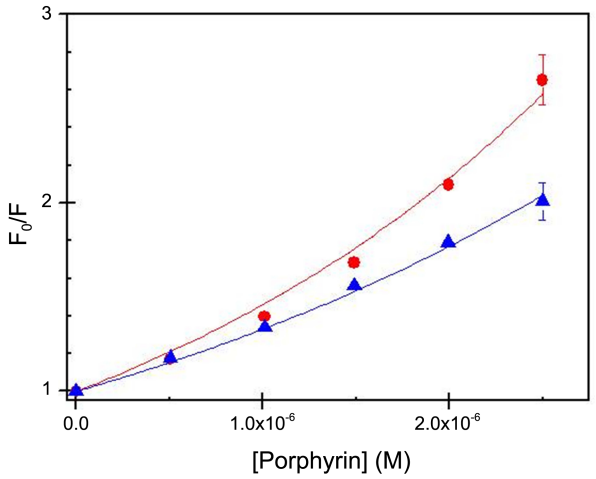

Figure 5. The Stern-Volmer plots constructed from the data in Figure 4. Red circles denote fluorescence quenching by TMPyP; blue triangles, BMPyP. The solid curves represent the best fits according to Equation (4).

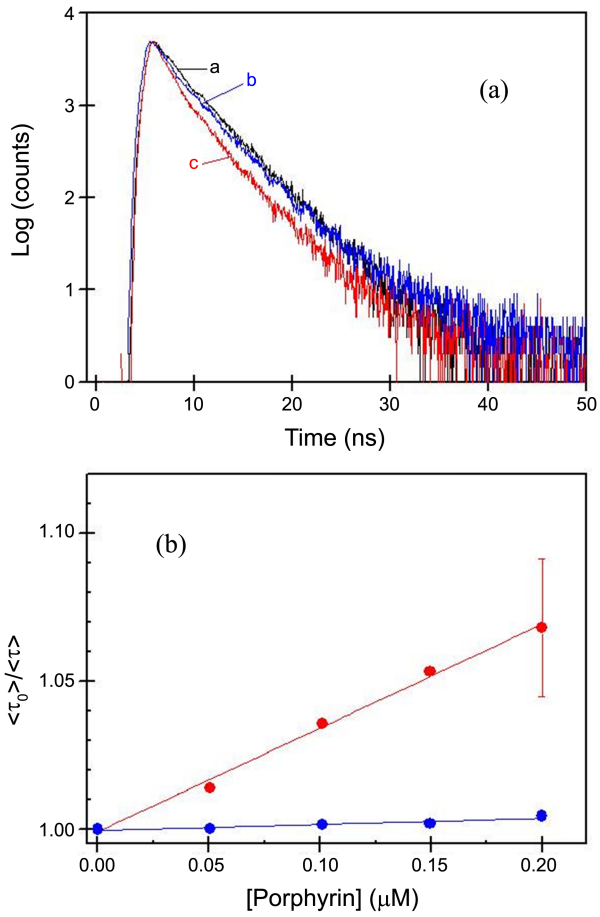

Figure 6. Panel a: Decay of fluorescence intensity of DNA-bound DAPI with respect to the time in the absence (curve a, black) and presence of BMPyP (curve b, blue) and TMPyP (curve c, red). [DNA] = 100 μM, [DAPI] = 0.5 μM and [TMPyP] = 2.5 μM. Excitation was at 360 nm and emission was at 450 nm. Panel b: Ratios of fluorescence decay times of DNA-bound DAPI in the absence and presence of TMPyP (red circle) and BMPyP (blue circle). The error bar represents the standard deviation from 4 measurements. The conditions for measurement are as in panel a.

plots' shapes suggest that the quenching mechanism was neither simple static nor dynamic-collisional.

Fluorescence Decay Times. Combined static and dynamic quenching can also results in upward bending Stern-Volmer plots. Dynamic quenching is expected to shorten the fluorescence decay time of the fluorophore. Fluorescence decay profiles of DNA-bound DAPI in the presence of TMPyP and BMPyP are compared in Figure 6(a). Fluorescence decay times of DNA-bound DAPI of 1.72 ns and 3.87 ns were observed in the absence of porphyrins with relative amplitudes of 0.129 and 0.871 respectively, in agreement with reported values.[37,38] BMPyP did not significantly alter the decay profile of the DNA-bound DAPI. TMPyP resulted in decay times of 1.33 ns and 3.67 ns with respective amplitudes, a_1 and a_2, of 0.393 and 0.607. The reduction of decay times by TMPyP reflect either the presence of DNA-bound TMPyP or the shortening of decay times through DAPI's interaction with TMPyP. The average decay time determined by $(a_1\tau_1^2+a_2\tau_2^2)/(a_1\tau_1+a_2\tau_2)$ was 3.22 ns in the presence of 2.5 mM TMPyP, indicating negligible dynamic contribution.[33] This was more clearly observable by plotting the ratio of the average decay times of DNA-bound DAPI in the absence and presence of TMPyP (Figure 6(b)). BMPyP had little effect on the decay time; 2.5 μM TMPyP reduced it by *ca.* 5%, showing that the fluorescence quenching had negligible dynamic contributions.

Overlap Integrals $J(\lambda)$. Although absorption in the Soret band is dominant, porphyrins absorb radiation over most of the UV/visible range, making them good acceptors for energy transfer. The fluorescence emission spectrum of DNA-bound DAPI overlapped with the absorption spectra of the porphyrins: normalized absorption spectra of the DAPI-DNA-TMPyP complex are shown in Figure 7; the fluorescence emission spectrum of DNA-bound TMPyP is also shown. Using BMPyP acceptor gave similar results. The overlap integrals (see below), $J(\lambda)$ correspond to the comm-

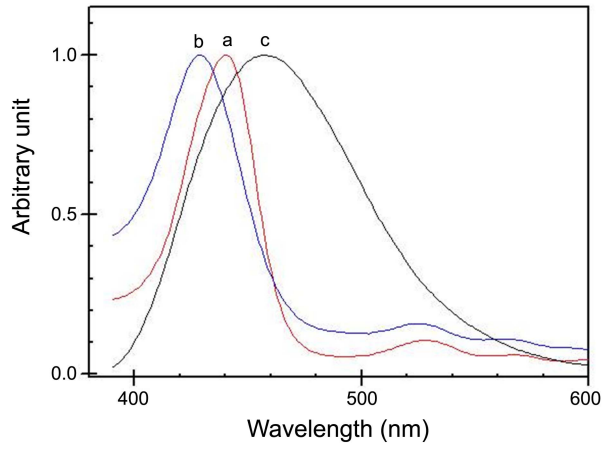

Figure 7. Rescaled absorption spectra of TMPyP (curve a, red) and BMPyP (curve b, blue) and the fluorescence emission spectra of DAPI (curve c, black), showing the spectral overlap when each porphyrin and DAPI bound to DNA simultaneously. Each spectrum was normalized to unity at its maximum.

on area under the emission spectrum of DAPI and the absorption spectra of the porphyrins. TMPyP showed a larger overlap integral than BMPyP: 10.102×10^{-13} cm^3mol^{-1} *vs.* 6.435×10^{-13} cm^3mol^{-1}. The quantum yield, Q_D of DNA-bound DAPI in the absence of porphyrins was calculated from the relative area of the respective emission spectrum.

Discussion

Inner Sphere Model and Energy Transfer Distance. Given the negligible change in the fluorescence decay time of DNA-bound DAPI in the presence of porphyrins, a simple combination of static-dynamic quenching could not account for the upward bending Stern-Volmer plots. An alternative mechanism to elucidate such quenching behavior is the "inner sphere model".

$$\frac{F_0}{F}=(1+K_D[Q])\exp([Q]VN/1000) \quad (2)$$

Where, K_D is the dynamic quenching constant, and V and N denote the volume of the sphere and Avogadro's number, respectively. The upward tending Stern-Volmer plot observed in the presence of TMPyP suggests the applicability of the inner sphere model (Equation (2)), with totally efficient quenching occurring when the fluorophore and quencher were within a certain distance (the sphere of action). In this equation, the dynamic quenching constant, $K_D=k_q\tau$, can be estimated from the ratios of the fluorescence decay time in the absence and presence of TMPyP at various concentrations. The fluorescence decay profiles of DNA-bound DAPI were described by a single exponential decay component; a short component appeared with increased TMPyP concentration, which was likely caused by the fluorescence decay of DNA-bound TMPyP, as a similar decay was observed in the absence of DAPI. Even if it were treated as a shortened DAPI decay time for the quenching of TMPyP, the averaged decay time remained constant, indicating a negligible contribution of K_D in Equation (2). This is plausible because both DAPI and porphyrin bound to DNA, preventing free collision between the two molecules. Therefore, Equation (2) could be reduced to Equation (3).

$$\frac{F_0}{F}=\exp([Q]VN/1000) \quad (3)$$

This equation was used to establish the best-fit curves to determine the radii of the spheres of action. The radius of the sphere of action corresponded to an implausible 1.58×10^6 bases for the DAPI-DNA-TMPyP complex because the quenching interactions were assumed to occur in 3-dimensional spheres in Equation (3), which is not the case for DNA-bound complexes. The DNA should be assumed to be a one-dimensional polymer for modeling the binding of the donor and acceptor. Using a 1-dimensional quenching model, Pasternack *et al.* proposed Equation (4) to describe the quenching behavior between DNA-bound donors and acceptors.[37]

$$\frac{F_0}{F} = \exp\left\{\frac{2\sigma[Q]}{[DNA]-2[D^{2+}]}\right\} \quad (4)$$

where $[Q]$ is the concentration of porphyrin quencher and $[D^{2+}]$ is the concentration of DAPI. σ denotes the minimum number of base-pairs between DAPI and the porphyrins required to permit energy transfer between them. The numbers of base-pairs calculated using equation (4) from the result in Figure 5 were 19.3 (66 Å) and 13.9 (47 Å) for TMPyP and BMPyP, respectively. DNA mediated fluorescence quenching is sometimes associated with electron transfer. However, this was not so here because the reduction potentials of porphyrins are generally high and the very short component of the donor's fluorescence decay time, which reflects the production of radical species, was not observed. Thus, the observed fluorescence quenching should be understood through the Förster-type resonance energy transfer without photon emission.

Resonance Energy Transfer Model. Förster-type energy transfer is based on the degree of transition dipole coupling. The distance at which RET is 50% efficient, R_0, is related to the spectral overlap between the emission spectrum of the donor and the absorption spectrum of the acceptor ($J(\lambda)$), the relative orientation of the transition dipoles of the donor and the acceptor (κ), the quantum yield of the donor in the absence of acceptor (Q_D), and the refractive index of the medium (n).

$$R_0=(J(\lambda)\kappa^2 Q_D n^{-4})^{1/6} \times 8.79 \times 10^{-25} \text{ in } cm \quad (5)$$

Where $J(\lambda)= \int_0^\infty F_D(\lambda)\varepsilon_A(\lambda)\lambda^4 d\lambda$ with $F_D(\lambda)$ denoting the normalized fluorescence intensity of the donor and $\varepsilon_A(\lambda)$, the molar extinction coefficient of the acceptor. The overlap integrals, $J(\lambda)$ in Equation (5), corresponding to the common areas under the emission spectrum of DAPI and the absorption spectra of the porphyrins, were estimated from Figure 7 to be 10.102×10^{-13} cm^3mol^{-1} and 6.435×10^{-13} cm^3mol^{-1} for TMPyP and BMPyP respectively. Within DAPI-TMPyP and DAPI-BMPyP cases, the Förster distances are $7.49 \times 10^7\kappa^{1/3}$ and $6.94 \times 10^7\kappa^{1/3}$ cm respectively.

In the Förster-type resonance energy transfer model, in addition to the distance between the donor and acceptor, their relative orientation also determines the efficiency of the energy transfer. Here the DAPI donor, bound at the minor groove of the DNA, had a fixed orientation. Differences in the binding geometries of the acceptors, TMPyP and BMPyP, resulted in different relative orientations. The binding modes of TMPyP and BMPyP to DNA and to selected synthetic polynucleotides has been investigated by polarized light spectroscopy,[34,35] with TMPyP found to intercalate between DNA base-pairs and BMPyP stackinf along the DNA stem. Therefore, their transition dipoles would be differently oriented relative to the DAPI. The orientation factor, κ^2, can range from 0 to 4,[33] depending on the relative orientation of the donor and acceptor molecules:κ^2=4 indicates parallel head-to-tail orientation and κ^2=1 indicates parallel orientation. However, varying κ^2 from 1 to 4 contributes to a difference in active distance of only 26% because the sixth root of this factor is considered (Equation 5). Therefore, the orientation factor cannot be the main factor leading to the observed difference in the energy transfer efficiency of TMPyP and BMPyP. The values obtained from both of the s and R_0 are the evidenced for higher fluorescence energy transfer of DAPI-TMPyP.

Conclusion

The energy of excited DAPI can transfer to cationic porphyrins across large distances when both are simultaneously bound to DNA. Overlap integrals ($J(\lambda)$) and the porphyrins' binding modes are at least in part responsible for the observed differences of RET efficiency.

Acknowledgments. This work was supported by the National Research Foundation (Grant no. 2011-0013534).

References

1. Núñez, M. E.; Barton, J. K. *Curr. Opin. Struct. Biol.* **2000**, *4*, 199-206.
2. Boon, E. M.; Barton, J. K. *Curr. Opin. Struct. Biol*. **2002**, *12*, 320-329.
3. Giese, B. *Curr. Opin. Chem. Biol*. **2002**, *6*, 612-618.
4. Wagenknecht, H.-A. *Angew. Chem. Int. Ed*. **2003**, *42*, 2454-2460.
5. Wagenknecht, H.-A. *Nat. Prod. Rep*. **2006**, *23*, 973-1006.
6. Murphy, C. J.; Arkin, M. R.; Jenkins, Y.; Ghatlia, N. D.; Bossmann, S. H., Turro, N. J.; Barton, J. K. *Science* **1993**, *262*, 1025.
7. Schuster, G. B. *Acc. Chem. Res*. **2000**, *33*, 253-260.
8. Giese, B. *Acc. Chem. Res*. **2000**, *33*, 631-636.
9. Takada, T.; Kawai, K.; Tojo, S.; Majima. T. *Tetrahedron Lett*. **2003**, *44*, 3851-3854.
10. Kawai, K.; Kodera, H.; Osakada, Y.; Majima, T. *Nature Chem*. **2009**, *1*, 156-159.
11. Lakhno, V. D.; Sultanov, V. B.; Pettitt, B. M. *Chem. Phys. Lett*. **2004**, *400*, 47-53.
12. Rak, J.; Makowska, J.; Voityuk. A. A. *Chem. Phys*. **2006**, *325*, 567-574.
13. Sadowska-Aleksiejew, A.; Rak, J.; Voityuk, A. A. *Chem. Phys. Lett*. **2006**, *429*, 546-550.
14. Murphy, C. J.; Arkin, M. R.; Ghatlia, N. D.; Bossmann, S.; Turro N. J.; Barton. J. K. *Proc. Natl. Acad. Sci. USA* **1994**, *91*, 5315-5319.
15. Núñez, M. E,; Noyes, K. T.; Barton, J. K. *Chem. Biol*. **2002**, *9*, 403-415.
16. Kelly, S. O.; Jackson, N. M.; Hill, M. G.; Barton, J. K. *Angew. Chem. Int. Ed*. **1999**, *38*, 941-945.
17. Vainrub, A.; Pettitt, B. M. *Chem. Phys. Lett*. **2000**, *323*, 160-166.
18. Park, S. J.; Taton, T. A.; Mirkin, C. A. *Science* **2002**, *295*, 1503-1506.
19. Porath, D.; Cuniberti, G.; Di Felice, G. R. *Charge Transport in DNA-based Devices*, In *Topics in Current Chemistry*; Vol. 237, Shuster, G. B., Ed.; Springer: Berlin, 2004; pp 183-228.
20. Lilley, D. M. J.; Wilson, T. J. *Curr. Opin. Chem. Biol*. **2000**, *4*, 507-517.
21. Murata, S.-I.; Kucœba, J.; Piszczek, G.; Gryczynski, I.; Lakowicz, J. R. *Biopolymers* **2000**, *57*, 306-315.
22. Kang, J. S.; Lakowicz, J. R. *J. Biochem. Mol. Biol.* **2001**, *34*, 551-558.
23. Malicka, J.; Gryczynski, I.; Fang, J.; Kusba, J.; Lakowicz, J. R. *Anal. Biochem*. **2003**, *315*, 160-169.
24. Lee, B. W.; Moon, S. J.; Youn, M. R.; Kim, J. H.; Jang, H. G.; Kim, S. K. *Biophys. J*. **2003**, *85*, 3865-3871.

25. Yun, B. H.; Kim, J.-O.; Lee, B. W.; Lincoln, P.; Nordén, B.; Kim, J.-M.; Kim, S. K. *J. Phys. Chem. B*. **2003**, *107*, 9858-9864.
26. Youn, M. R.; Moon, S. J.; Lee, B. W.; Lee, D.-J.; Kim, J.-M.; Kim, S. K. *Bull. Korean Chem. Soc*. **2005**, *26*, 537-542.
27. Choi, J. Y.; Lee, J.-M.; Lee, H.; Jung, M. J.; Kim, S. K.; Kim, J.-M. *Biophys. Chem*. **2008**, *134*, 56-63.
28. Jin, B.; Lee, H. M.; Lee, Y.-A.; Ko, J. H.; Kim, C.; Kim, S. K. *J. Am. Chem. Soc*. **2005**, *127*, 2417-2424.
29. Jin, B.; Min, K. S.; Han, S. W.; Kim, S. K. *Biophys. Chem*. **2009**, *144*, 38-45.
30. Larsen, T. A.; Goodsell, D. S.; Cascio, D.; Grzeskowiak, K.; Dickerson, R. E. *J. Biomol. Struct. Dyn.* **1989**, *7*, 477-491.
31. Vlieghe, D.; Sponer, J.; Van Meervelt, L. *Biochemistry* **1999**, *38*, 16443-16451.
32. Kim, H.-K; Kim, J.-M.; Kim, S. K.; Rodger, A.; Nordén, B. *Biochemistry* **1996**, *35*, 1187-1194.
33. Lakowiz, J. R. *Principles of Fluorescence Spectroscopy*; 3rd ed. Springer, New York, 2006; pp 443-472.
34. Jin, B.; Ahn, J. E.; Ko, J. H.; Wang, W.; Han, S. W.; Kim, S. K. *J. Phys. Chem. B*. **2008**, *112*, 15875-15882.
35. Lee, Y.-A.; Lee, S.; Cho, T.-S.; Kim, C.; Han, S. W.; Kim, S. K. *J. Phys. Chem. B*. **2002**, *106*, 11351-11355.
36. Ismail, M.; Rodger, P. M.; Rodger, A. *J. Biomol. Struct. Dyn.* **2000**, *Conversation 11*, 335-348.
37. Cavatorta, P.; Masotti, L.; Szabo, A. G. *Biophys. Chem.* **1985**, *22*, 11-16.
38. Szabo, A. G.; Krajcarski, D. T.; Cavatorta, P.; Masotti, L.; Barcellona, M. L. *Photochem. Photobiol.* **1985**, *44*, 143-150.
39. Pasternack, R. F.; Caccam, M.; Keogh, B.; Stephenson, T. A.; Williams, A. P.; Gibbs, E. J. *J. Am. Chem. Soc*. **1991**, *113*, 6835-6840.